GEOLOGICA BELGICA (2007) 10/1-2: 109-119

PRODUCTION OF A MATRIX-MATCHED STANDARD FOR QUANTITATIVE ANALYSIS OF IRON SULPHIDES BY LASER ABLATION INDUCTIVELY COUPLED PLASMA-MASS SPECTROMETRY BY WELDING: A PILOT STUDY

Stijn DEWAELE[1,2], Philippe MUCHEZ[2] & Jan HERTOGEN[2]

(6 figures and 4 tables)

[1.] *Department of Geology and Mineralogy, Royal Museum for Central Africa, Leuvensesteenweg 13, 3080 Tervuren. E-mail: stijn.dewaele@africamuseum.be*
[2.] *Geodynamics & Geofluids Research Group, K.U.Leuven, Celestijnenlaan 200E, 3001 Leuven, Belgium.*

ABSTRACT. Over the recent years, several laboratories have tried to solve the matrix-match problem for quantitative analysis of sulphides with Laser Ablation Inductively Coupled Plasma Mass Spectrometry (LA ICP-MS) by developing artificial standards. This paper investigates the feasibility of a modified welding technique for the production of artificial sulphide crystals as a matrix-matched external standard for quantitative analysis of the trace element content of natural samples with LA ICP-MS. During this research, focus was on pyrite, since this mineral phase is an ubiquitous mineral in several ore deposits and sedimentary/diagenetic successions. The matrix-matched standard has been produced by resistance heating of a µm-size mixture of pyrite and pure elements in graphite electrodes with a procedure modified after Ødegard (1999). During the loss of S during the welding, the formed bead consists of pyrrhotite. Pyrrhotite, however, exhibits similar ablation behaviour as pyrite. For several elements of interest (i.e. Co, Ni, Cu and Ga), the matrix-matched standard shows a homogeneity ≤ 15 % RSD, which is sufficient for a (semi-)quantitative calibration. Some elements (i.e. Zn, Se and Pb) show a rather poor homogeneity (RSD ≥ 15 %), which only allows a qualitative analysis. The concentration of Ge and As is below the detection limit in the produced standards, which can be due to vaporisation during welding or during ablation of the beads. The obtained homogeneity is comparable to most of matrix-matched LA ICP-MS sulphide standards described in the literature. The use of the matrix-matched standard has been illustrated on hydrothermal pyrite from a mesozonal orogenic mineralisation (Marcq area, Belgium), which has been analysed as well with the electron microprobe. Owing to the higher sensitivity many more trace elements can be measured with LA ICP-MS. The LA ICP-MS analyses clearly demonstrate a variation of trace element content and enrichment of the elements (Cu, Pb, Zn, Se) towards the rim of the pyrite crystal.

KEYWORDS: LA ICP-MS, matrix-matched standard, Fe-sulphides, welding device.

1. Introduction

Pyrite (FeS_2) is the most abundant sulphide mineral in the earth's crust and is ubiquitous in different types of mineralisation (Craig *et al*., 1998) and sedimentary/diagenetic deposits. It is formed during different stages in the evolution of a sedimentary basin, from the early diagenetic stage until the final metamorphic conditions within an orogeny, and during magmatic processes. Pyrite and other associated sulphides can precipitate from different fluid types that circulate through a sedimentary basin. Magmatic, metamorphic and basinal fluids, seawater and modified meteoric water can be considered as possible sources of sulphides. Because pyrite is a refractory mineral, it retains many characteristics (e.g. geochemistry and morphology) even during penetrative deformation (Craig *et al*., 1998; Foley *et al.*, 2001) and metamorphism up to amphibolite facies (Parr, 1994). During crystallization/growth of the mineral, different elements can be incorporated in its structure. Therefore, it may provide valuable information about the changing physico-chemical conditions during burial and metamorphism. Due to the presence of pyrite associated with many types of mineralisation, its minor element composition is commonly studied to unravel the origin and the physico-chemical conditions of the mineralising fluids (e.g. Ryall, 1977; Bralia *et al*., 1979; Duchesne *et al*., 1983; Griffen *et al*., 1991; Fleet *et al*., 1993; Huston *et al.*, 1995; Raymond, 1996; Fleet & Mumin, 1997). Different techniques can be used separately or in combination to characterize the chemical composition of pyrites, though electron microprobe techniques are most commonly used (Robinson *et al*., 1998). The present study focuses on Laser Ablation Inductively Coupled Plasma-Mass Spectrometry (LA ICP-MS).

LA ICP-MS is considered to be a powerful tool for in-situ analysis of minerals due to its wide element coverage and low detection limit (cf. Ridley & Lichte, 1998). However, elemental analysis by laser sampling suffers from a complex relationship between signal and concentration due to the variable amount of material ablated and entrained in the ICP-MS. This problem is

largely solved by rationing the measured signals of the elements of interest against an internal standard, i.e. a mineral phase containing the latter element with a known concentration. The behaviour of the internal standard during ablation should be representative of those elements for which a calibration is sought (Jarvis & Williams, 1993). The internal standard and the analyte should have a similar mass and should be close in boiling point and ionisation potential (Ridley & Lichte, 1998). The intensity ratios are calibrated to obtain a response ratio (counts per second / ppm), using an external standard with known concentrations of trace elements. However, the lack of suitable external calibration materials is a common and serious problem in quantitative microanalysis. Calibration materials must be homogeneous at the small scale of resolution at which the technique will be used. In addition, the calibration material should preferentially have a matrix that closely matches the samples to be analysed, both chemically and physically. Furthermore, these materials must have certified or reliable working values for the contents of all the elements of interest (Ødegard, 1999).

Due to the lack of suitable sulphide standards, the NIST SRM 612 and 614 glasses are commonly used for calibration (e.g. Campbell & Humayan, 1999; Arif & Baker, 2004; Halter *et al*., 2004). However, these standard glass reference materials with known compositions have different ablation behaviours than sulphides due to a different matrix (Ridley & Lichte, 1999). Many attempts have already been made to produce matrix-matched standards for sulphides. Axelsson (2000), Axelsson & Rodushkin (2001) and Müller *et al*. (2002) searched for natural homogeneous sulphide crystals. Because homogeneous standards for minor elements are very rare (or can not be found), other research groups have tried to produce sulphides artificially. Perkins *et al*. (1997) used pressed pellets of µm-sized pyrite. However, these pellets have different ablation behaviour. A recent study reported the use of borate glasses spiked with sulphides as LA ICP-MS standards for sulphides (Norman *et al*., 2003). Ballhaus and Sylvester (2000) described a method to produce $Fe_{1-x}S$ standards for PGE elements, by heating a FeS-S mixture, spiked with elements of interest, in a silica tube at 950°C. Nesbitt *et al*. (1997) used an artificial NiS standard for the analysis of PGE elements in sulphides. Wilson *et al*. (2002) created an artificial sulphide standard that seems to be accepted amongst the geochemistry

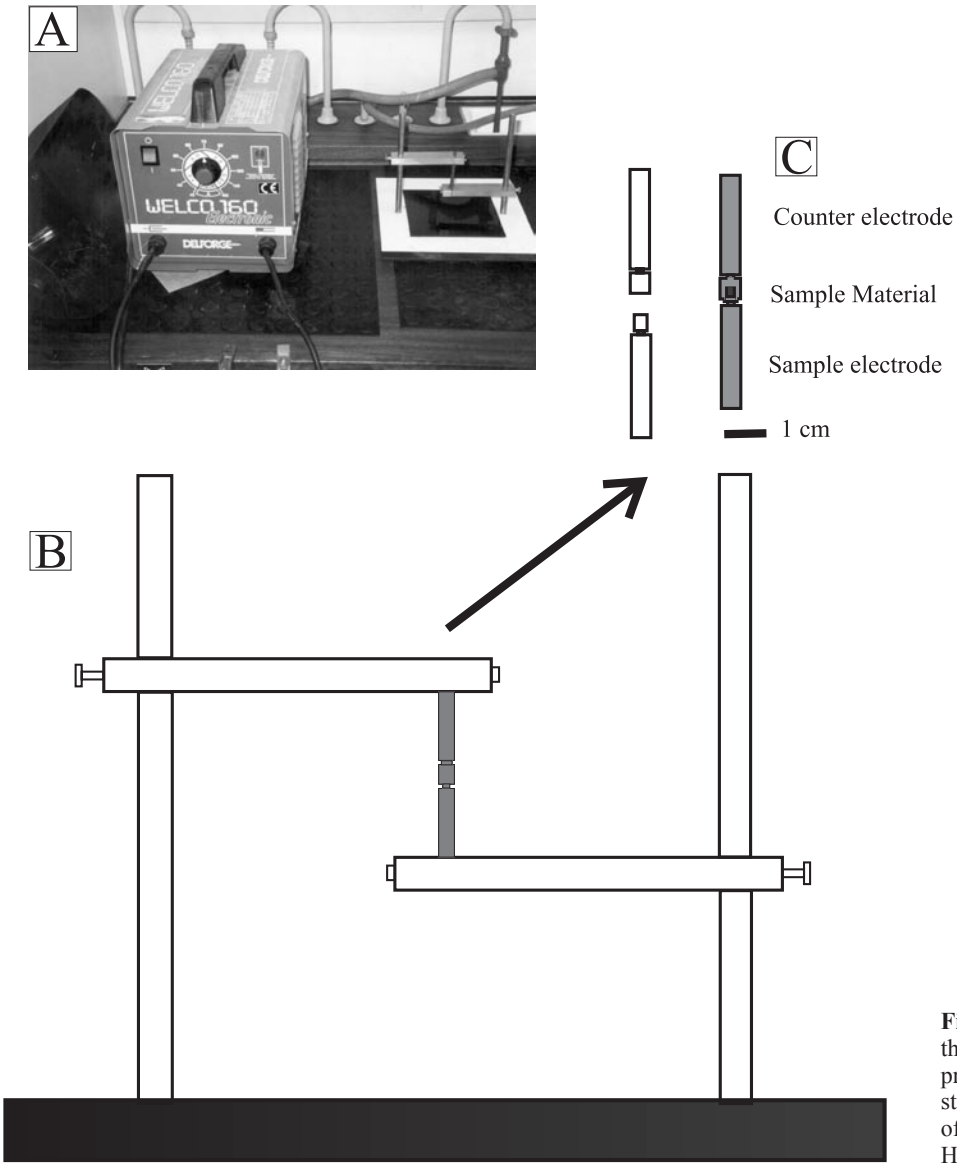

Figure 1. A. Photograph showing the experimental set-up for the production of artificial sulphide standards. B. Detailed reconstruction of experimental configuration. C. High-purity graphite electrodes.

community. This amorphous standard is produced by the precipitation of sulphides in solution. However, the aliquots of the standard material are crushed and pressed in as pellet before laser ablation and, therefore, exhibit different ablation behaviour as natural sulphides occurring as crystals.

In the present study, a welding method was tested to produce homogeneous matrix-matched crystalline sulphide standards for the LA ICP-MS analysis of the trace element content of natural Fe-sulphides. Pyrite was selected as application since its ubiquitous occurrence. The quantitative LA ICP-MS method has been tested on pyrite from a mesozonal polysulphide mineralisation in the Anglo-Brabant fold belt in Belgium, for which electron microprobe data is available (Dewaele *et al*., 2002b; Dewaele & Muchez, 2005).

2. Methodology

2.1 Experimental set-up

Pyrite standards were made by modifying the Ødegard method (1999), which was successful for rare earth element analysis in quartz and rutile. The method is based on direct fusing in high-purity graphite electrodes by resistance heating with a welding rectifier as the power device (Figure 1A). The sample is placed between a lower sample electrode and a higher counter electrode (Figure 1B & C). The welding device used as a Welco Electronic 160, with a current range between 40 to 150A. The electrodes are made of high-purity, chemically inert graphite (Figure 1C, Electrode-Crater, U7/SPK, Carbone Lorraine), which greatly reduces the risk of contamination. The graphite also limits oxidation during welding. The mineralogy of the resulting beads is confirmed by X-ray diffraction. The poles of the set-up are connected to the poles of the welding device. An electrical current generates resistance heating in the electrodes, which causes the melting of the powder sample between the electrodes. The advantage of the experimental configuration applied is the rapid and efficient heating and melting and the short quenching time. However, the welding device used does not allow to control the output current sufficiently. This limits the control on the temperature generated and the reproducibility of the production process. Due the lack of control on the temperatures, it is impossible to determine exactly the equilibrium temperatures that are reached during welding.

The starting material for the experiments is a pyrite sample from Elba Island, taken from the in-house mineralogical collection. This pyrite is commonly used as an electron microprobe standard (oral communication Jacques Wautier). Macroscopic, microscopic investigation and XRD-analysis of this pyrite did not show the presence of other sulphides and growth zoning. In a first step, the pyrite was crushed to a µm-grain size in a Phillips PW4018/00 MiniMill. This MiniMill typically produces powders with a µm-grain size (average grain size 2 µm). One gram of pyrite powder was spiked with small amounts of µm-grain size powder (~ 0.01 g) of the pure elements of interest (As, Co, Ni, Cu, Zn, Pb, Ga, Ge, Se), taken from the in-house mineralogical collection. These elements were added to increase the trace or minor element content of the artificially made sulphides, since the Elba pyrite has very low contents of trace or minor elements. This low content of trace or minor elements of the Elba pyrite was indicated by preliminary LA ICP-MS analysis, which did not show counts per second above the background level for most of the trace or minor elements. The exact composition of the Elba pyrite is not determined. Additional sulphur (0.3 g) was added to compensate for the loss of sulphur during melting and to prevent exsolution during rapid cooling (e.g. Ballhaus and Sylvester, 2000). Preliminary experiments showed that welding of pyrite - and even pyrrhotite- without the addition of extra sulphur resulted in the formation of pure iron and minor sulphides, as was illustrated by microspcopy and XRD analysis (Fig. 2). A bigger amount of As (0.1g) was added to the mixture since arsenic is an important element for the geochemistry of pyrite. Furthermore the presence of As can influence the crystal structure of pyrite during crystallisation (Ramdohr, 1969), which could allow the incorporation of a higher amount of trace elements. For 24h, the mixture was mixed using a magnetic stirring table. All grinding and mixing occurred in isopropanol to avoid oxidation. Finally, small amounts of the sulphide and pure elements mixture (~100 mg) were inserted in the electrodes.

A commercially available LSX200 Laser Ablation System (Cetac Technologies, Inc.) is used. Experimental conditions are listed in Table 1. This system consists of a frequency-quadrupled Nd:YAG laser. The ablation cell is mounted on a motorized and software controlled XYZ

ICP-MS (HP4500)		
carrier gas flow (l/min)	Ar	1.3
	He	/
auxilliary gas flow (l/min)		1
plasma gas flow (l/min)		14.9
RF-power (W)		1300
mass resolution (AMU)		~0.3
analysis method		time resolved analysis
measured isotopes		^{57}Fe, ^{59}Co, ^{60}Ni, ^{63}Cu, ^{66}Zn, ^{69}Ga, ^{72}Ge ^{75}As, ^{82}Se, ^{208}Pb
number of points per peak		1
sampling period (s)		3.15
Integration time (s)	^{57}Fe	0.035
	^{59}Co	0.1
	^{60}Ni	0.4
	^{63}Cu	0.035
	^{66}Zn	0.11
	^{69}Ga	0.035
	^{72}Ge	0.95
	^{75}As	0.11
	^{82}Se	0.5
	^{208}Pb	0.035

Laser (Cetac LSX200)	
wave length (Nm)	266
pulse duration (ns)	< 6
energy level	10
repetition rate (Hz)	5
burst count	100
output energy (mJ)	< 5
spotsize (µm)	50
ablation method	single point

Table 1. Experimental parameters of LA ICP-MS and ablation system.

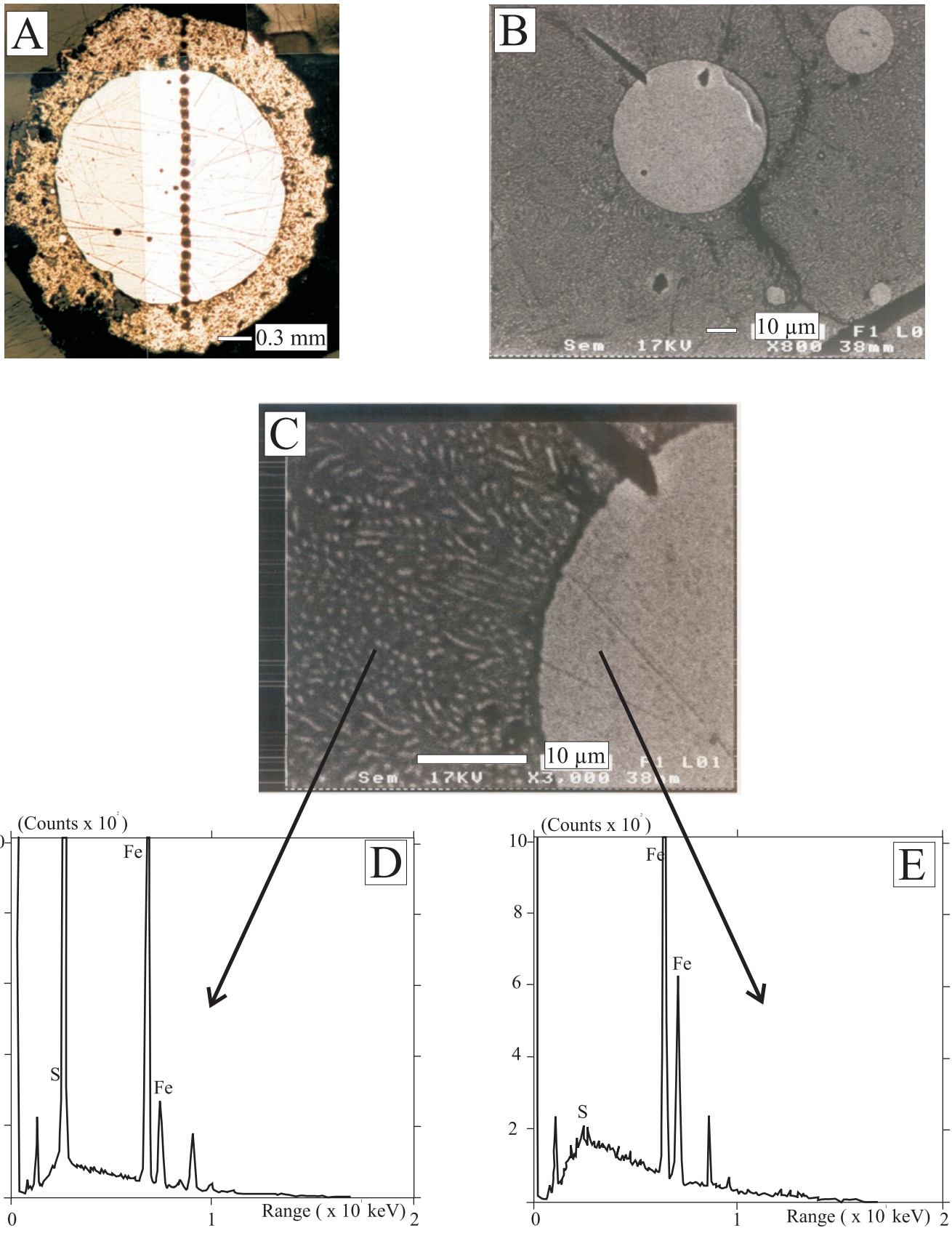

Figure 2. A. Photograph of polished section showing a white coloured central core, consisting of iron, surrounded by a darker coloured rim, consisting of pyrrhotite and exsolved iron. B & C. Backscatter image of an exsolution texture iron-pyrrhotite. Dark phase is pyrrhotite, while white phase is iron. The white rounded phase is a big droplet of iron. This white-coloured phase also occurs as exsoluted phase between the darker coloured pyrrhotite in the left part of the picture. D. EDX-spectrum of the dark-coloured phase, i. e. pyrrhotite. E. EDX-spectrum of the white coloured phase, i.e. iron.

table. Samples and the ablation processes can be viewed with a CCD camera. Typical for the laser is the homogeneous energy distribution, the so-called "flat topped beam profile". The laser system has a maximum pulse energy on the sample of ~ 5 mJ; the repetition rate can be varied between 1 and 20 Hz. The measurements have been carried out with an Agilent HP4500 ICP-MS, operating in time resolved analysis mode. The measurement conditions are summarized in Table 1. By shooting series of single points, the homogeneity of the beads was tested by comparing the ratios of the measured signals of the elements of interest against the internal standard ^{57}Fe and calculating the relative standard deviation (%RSD). At least 50 points in different trails were shot in different directions across the entire bead. To avoid saturation of the ion detector, the mass spectrometer was not tuned for maximum sensitivity and the integration time was lowered for ions, which generally caused the detector signal saturation (^{57}Fe and ^{63}Cu). Typical sensitivity setting produced ca 15000 cps ^{59}Co for the 10 ppm Co standard. Before every set of analysis, the ICP-MS was tuned with the NIST 612 standard to the same sensitivity, to obtain a certain reproducibility between different measurements.

2.2 Results of welding experiments

Various procedures were tested for the production of the most homogeneous bead. The homogeneity of each of the produced beads was tested by microscopic investigation, followed by LA ICP-MS investigation. One procedure consists of a degassing step, a melting step and a "controlled" cooling step. During the initial step, the sample was heated to remove gases of isopropanol (used for cleaning), H_2O, CO_2, etc. Tests showed that at least 60 sec at the lowest available current (40A) was necessary to remove all the gases. This step only produces an aggregate of sintered pyrite grains with little cohesion. During the second step in the procedure, the main melting takes place. Several experiments have been undertaken to define the most effective melting conditions. Different currents (60 A – 75 A – 90 A – 100 A – 120 A) with different heating time intervals (15 sec – 30 sec – 45 sec – 60 sec) were tested. During this melting step, several problems were encountered. Firstly, X-ray diffraction showed that the resulting product was not pyrite but mainly pyrrhotite. However, reported experiments indicated similar ablation behaviour for pyrrhotite as for pyrite (cf. Watling *et al*., 1995). Different ablation tests on Elba pyrite and the pyrrhotite beads in the laboratory indeed showed that ablation resulted in a comparable ablation crater morphology and a comparable quantity of effective counts per second for both sulphides. Therefore the pyrrhotite standard is considered suitable as pyrite standard. A second problem is phase separation. XRD and SEM analysis indicate that iron metal exsolves from pyrrhotite when applying a high current (starting from heating at 90 A, Fig 2A,B,C). At 743°C, pyrite incongruently melts to hexagonal pyrrhotite and an almost pure sulphur fluid (Kullerud & Yoder, 1959). At about 1200°C, melting of pyrrhotite results in a mixture of a liquid and a gas phase (Fig. 3; Kullerud & Yoder, 1959). Due to our experimental set-up, we have a continuous loss of gases (sulphur) during heating of the samples, resulting in blebs of pure iron next to pyrrhotite. By heating the samples too long and applying a too high of a current, created samples consistently had a composition falling in the stability field of a mixture of iron and pyrrhotite (Fig. 3), characterized by an exsolution texture or even pure iron beads (Fig. 2A,B,C; dotted line in Fig. 3). Therefore, the most homogeneous pyrrhotite crystals were obtained after welding at a current of only 75A for a time period of at least 45 seconds. If welding was done for a time period of more than 75 seconds, the bead dominantly consisted of iron (Fig 2A). It should be noted that even in the theoretical case of no loss of sulphur during melting (dotted light grey arrow in Fig. 3), the resulting bead would be pyrrhotite instead of pyrite due to the slow transformation of pyrrhotite to pyrite (Kullerud & Yoder, 1959).

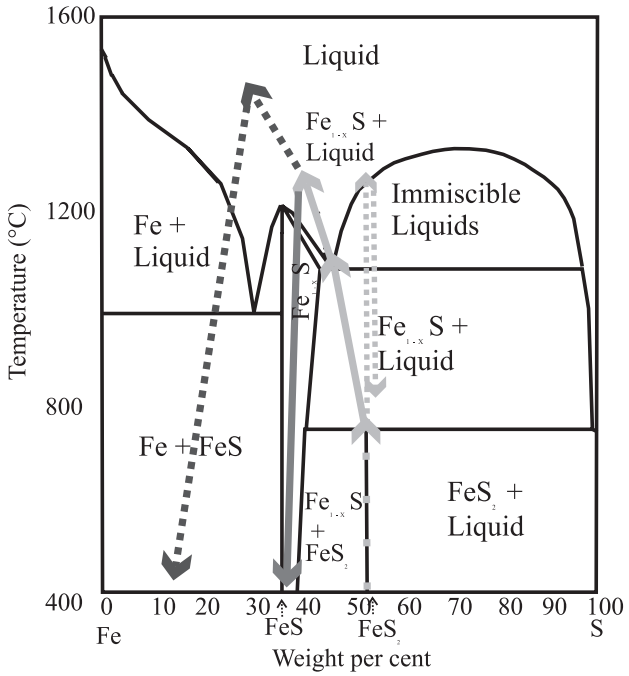

Figure 3. Phase stability field of the Fe-S system (after Kullerud & Yoder, 1959). Light grey arrow illustrates phase transitions during heating, whereas dark grey arrow indicates transitions during "controlled" cooling of the standard. Dotted line shows presumed transitions during melting at too high current for a too long period. Dotted light grey arrow illustrated phase transitions in the theoretical case of no loss of sulphur during melting.

The standard procedure was optimised to create the most homogeneous sulphide standard. Experimental results showed that a better control on the resulting bead was obtained by introducing a third step in the process, i. e. a controlled cooling step to prohibit rapid quenching. During quenching, the vapour bubbles were not able to escape, resulting in large cavities in the standards (up to 1 mm in a standard of 3 mm). During the cooling step, the standard is kept at a lower moderate current for some period. Increasing the duration of the third step reduced the amount of fractures, bubbles and resulted in a more homogeneous sample. Several experiments resulted in apparently homogeneous standards (Fig. 4A) after a degassing step of 60 sec at 40A, a welding step of 50 sec at 75A and a cooling step of 60 sec at 60A. The standard

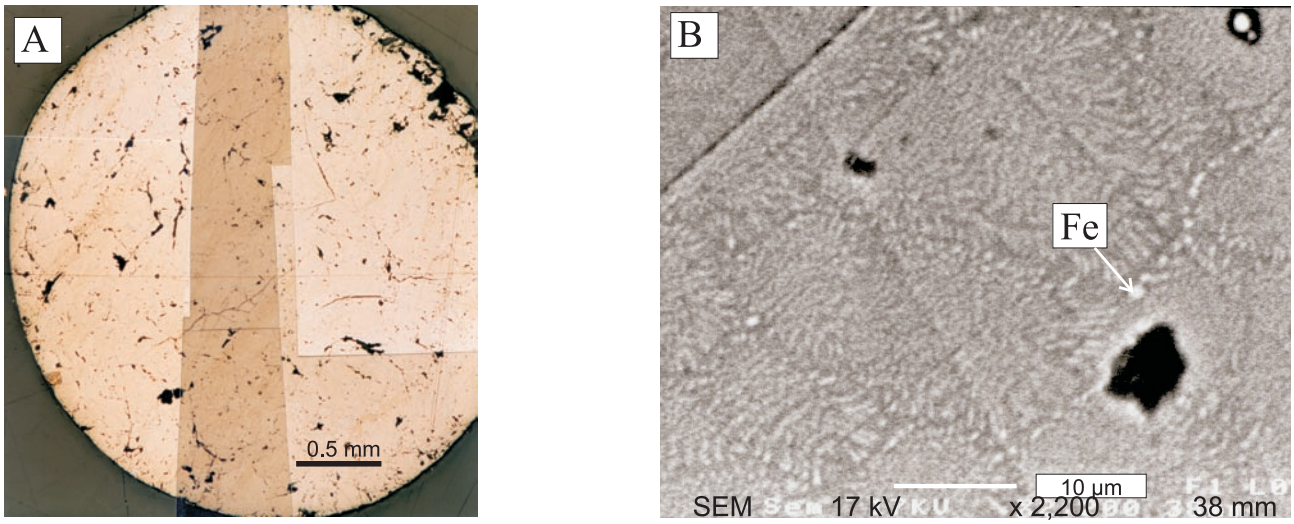

Figure 4. A. Composite photograph showing polished section of homogenous light yellow-brown bead. B. Photograph of backscatter SEM showing µm-scale iron inclusions (white) in pyrrhotite (greyish). The cracks and holes in both pictures are formed during the cooling of the samples.

is identified as hexagonal pyrrhotite by XRD analysis (dark grey arrow in Fig. 3). However, backscatter SEM analysis indicates the presence of sub-µm inclusions of iron (Fig. 4B).

The welding experiment was repeated several times, to test the reproducibility of the experiment. Petrographic investigation and SEM-analysis revealed that the different beads produced had a comparable homogeneity.

	A Sample GI4 RSD(%)	B Trace element GI4 (ppm)	C detection limit LA ICP-MS (ppm)
Co	5	1147	10
Ni	9	109	20
Cu	5	1240	10
Zn	35	448	5
Ga	11	588	15
Ge	65	5	10
As	<100	16	80
Se	18	54	50
Pb	22	490	10

Table 2. A. Homogeneity of standard GI4, reported in relative standard deviation of the effective counts normalized against effective counts of Fe^{57} (%RSD). B. Trace element concentration in the standard, as measured with standard solution ICP-MS. C. Detection limit of trace element content by LA ICP-MS, determined by combining 3–σ, effective counts and effective concentration of the elements in the standard.

2.3 Analysis artificial standard

2.3.1 Microanalysis

Homogeneity of the elements in the artificial standards is reported as the relative standard deviation of the ratio of normalized counts per second of the elements versus the counts per second of Fe^{57} (%RSD, Table 2A). The %RSD is calculated based on least 50 points, shot in different trails in different directions on the entire bead. For several elements of interest (Co, Ni, Cu and Ga) homogeneity was better than 15 percent. The homogeneity is not good (i.e. RSD > 15%) for Zn, Ge, Se and Pb. Very unfavourable results are obtained for As (i.e. a RSD > 100%), with effective counts per second varying above and below the background. This could be explained by the loss of As during melting of the pyrite powder and ablation of the standards. Also, the response for Ge is locally below the background, which could also be explained by the volatilisation of Ge during melting or during ablation. A relative standard deviation < 15 percent indicates that the standard is suitable for a (semi-) quantitative analyses of pyrite. Similar homogeneities are described for artificial external standards in other LA ICP-MS studies (Jarvis & Williams, 1993; Axelsson, 2000).

It should be noted that the measured concentrations in the artificially produced beads are much lower than the amount of elements that has been added to the mixture of µm-grain size pyrite and the pure elements. No investigation has been carried out to explain this, since it is not the real scope of this article. But the loss of the minor or trace elements could probably be due to loss during the welding of the mixture pyrite and pure elements or due to fractionation during ablation.

2.3.2 Bulk analysis

The chemical composition of the standards has been determined by solution ICP-MS, after dissolving the pyrite standards with the three acids HCl-HNO_3-$HClO_4$ (Table 2B). The detection limit for LA ICP-MS of the standards has been calculated using 3-σ (= 3 times the standard deviation), the concentration and the normalized counts for each element in the artificial standard (Table 2C). The normalized counts per second and the concentration for each element are combined to calculate the correction factors for each element. Problems arise for As and Ge since the concentration of these elements in the standard is often too low to analyse with LA ICP-MS. Although there are no direct indications, it is possible that these elements are lost during the melting of the powders.

3. Illustration

3.1 Marcq area mineralisation

The artificial standard has been applied to the analysis of pyrite from the mesozonal orogenic polysulphide mineralisation in the Marcq area, Belgium (Piessens *et al.*, 2002; Dewaele *et al.*, 2002a). The Marcq mineralisation is associated with a shear zone at the southern margin of the Lower Palaeozoic Anglo-Brabant fold belt in Belgium and resulted from the migration of metamorphic fluids during the Late Silurian to Early Devonian Brabantian orogeny. The polysulphide mineralisation occurs disseminated in the host rock or concentrated in veins, and is associated with an intense sericitisation, chloritisation and silicification. The paragenesis can be summarized in four stages (Piessens *et al.*, 2002; Dewaele *et al.*, 2002a). The earliest sulphides (stage 1) are framboidal pyrites that formed during early diagenesis. The first veins, consisting of pyrite (stage 2), are a few millimetres thick and precipitated along (initial) cleavage or parallel to bedding planes. These stage 2 veins are considered as the initial phase of the tectonometamorphic phase of the mineralisation (Piessens *et al*. 2002). Stage 3 is characterized by mineralised quartz veins, which commonly occur along weakly dipping cleavage planes. The mineralisation dominantly consists of pyrite, pyrrhotite, marcasite, arsenopyrite, galena, chalcopyrite, sphalerite and stibnite (Piessens *et al*., 2002; Dewaele *et al*., 2002a). This phase is considered as the main mineralising event. Finally, quartz and pyrite precipitated in subvertical extension veins, without any evidence of deformation along vein walls (stage 4).

An electron microprobe investigation has been carried out on different pyrite generations (Dewaele *et al*., 2002b; Dewaele & Muchez, 2005). Due to the limited number of measurements within the 3-σ confidence level (99.7 % confidence level, cf. Robinson *et al*., 1998), comparison among the different pyrite generations was based on the percentage of significant measurements for each element (cf. Eilu *et al*., 1997). The investigation illustrated an increase of significant measurements for the elements As, Co, Se, Au and Sb in stage 3, compared to pyrites present in early and later pyrite. Experimental parameters of electron microprobe analysis are given in Table 3.

Electron microprobe	
beam current (nA)	100
acceleration voltage (kV)	20
LIF	Fe, Co, Ni, Cu
TAP	Zn, As, Se
PET	S, Pb, Au
PET	Sb, Cd, Te
measurement time (s)Fe, Co, Ni, Cu	20
Zn, As, Se	26
S, Pb, Au	26
Sb, Cd, Te	26

Table 3. Experimental parameters used during electron microprobe analysis.

3.2 Results LA ICP-MS analysis of mesozonal pyrite

Pyrite has been selected from stage 2 of the Marcq mineralisation (sample 14200B8) for detailed LA ICP-MS analysis. This pyrite generation formed contemporaneously with cleavage development during the initial phase of the tectonometamorphic deformation, but before the main polysulphide mineralisation phase associated with quartz veining. Etching of the syn-tectonic pyrites revealed µm-scale zoning (Fig. 5A and B), indicative of changing physico-chemical conditions during growth of the pyrite crystals (Shore and Fowler, 1996). Based on the presence of growth zoning and the paragenetic position (just before the main mineralisation), the pyrite from stage 2 was selected to investigate the possible changing geochemistry towards the main stage of the mineralisation (i.e. stage 3).

An electron microprobe study (n = 13 points) resulted in low percentages of significant measurements for most of the trace element (Table 4A). Therefore, for calculation of average values, contents at half of the detection limit were used for measurements falling outside the 99.7 percent confidence level. This severely limits the possibility of comparing the results of electron microprobe and LA ICP-MS. The minimum, maximum, average, median and the percentage of significant measurements are indicated in Table 4A. Electron microprobe analysis commonly results in high maximum values, whereas the

	minimum	maximum	**average**	**median**	% significant measurements		minimum	maximum	**average**	**median**	% significant measurements
	A	Electron microprobe					B	LA ICP-MS			
Co	bd	bd	bd	bd	Ns	Co	bd	808	**225**	**153**	95
Ni	bd	600	**266**	**250**	54	Ni	37	5656	**1027**	**523**	100
Cu	bd	5600	**560**	**bd**	23	Cu	bd	1353	**165**	**61**	90
Zn	bd	800	**200**	**bd**	31	Zn	22	244	**49**	**32**	100
Ga	Nm	Nm	**Nm**	**Nm**	Nm	Ga	bd	131	**34**	**26**	80
As	200	14892	**3184**	**2000**	100	As	bd	25186	**5873**	**2702**	95
Se	bd	5000	**608**	**300**	61	Se	111	1480	**620**	**522**	100
Ag	bd	1500	**390**	**bd**	38	Ag	Nm	Nm	**Nm**	**Nm**	10
Pb	bd	9900	**1246**	**bd**	38	Pb	bd	462	**79**	**31**	90

Table 4. Comparison between the results obtained by LA ICP-MS (B) and electron microprobe analysis (A). Nm = not measured, Ns = non-significant and bd = below the detection limit. Detection limit for electron microprobe was ~ 200 ppm for most elements. Ge was not analysed by electron microprobe. The percentage of significant measurements was calculated by rationing the number of measurement above the detection limit versus the total number of measurements.

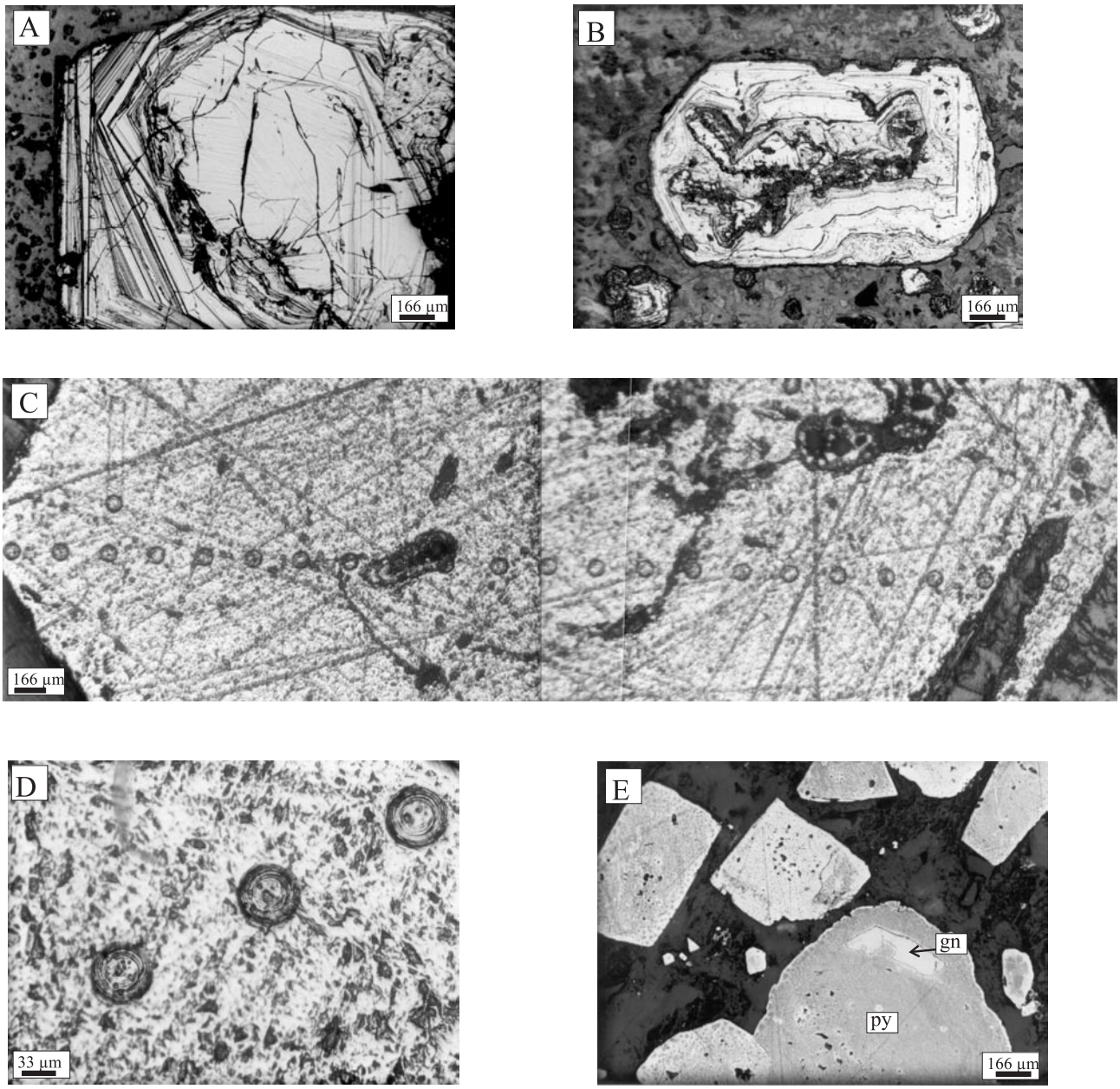

Figure 5. A & B. Photograph showing intensely zoned pyrite crystal from mineralisation stage 2. Pyrite has been etched by using a mixture of equal amounts of 0.1 M $KMnO_4$ and 0.1 M H_2SO_4. C. Photograph showing 23 spots shot across pyrite crystal in sample 14200B8. D. Ablation spots of 50 µm in sample 14200B8. E. Photograph showing inclusion of galena (gn) parallel to a crystal growth plane in pyrite (py) from stage 2.

median values fall below the detection limit (Co, Cu, Ag, Zn and Pb). The high maximum values could be explained by the analysis of sub-microscopic sulphide inclusions, present in the pyrite crystal (cf. Huston *et al*., 1995).

A trail of 23 points was analysed by LA ICP-MS from one corner to another in the regularly zoned pyrite crystals (Fig. 5 C and D). For most elements, the LA ICP-MS analysis yielded percentages of significant measurements better than 80 percent, which are a significant improvement compared to electron microprobe analysis (Table 4B). Although a direct comparison of the two data sets is not feasible due to the low percentage of significant measurements from the electron microprobe, it can be noted that the maximum and median values for different elements are comparable (Table 4). Also, if the median value obtained by electron microprobe is below the detection limit (i.e. ~ < 200 ppm), an average value below 200 ppm is obtained by LA ICP-MS analysis.

LA ICP-MS analysis shows symmetric variation for the elements Co and Ni from core to rim (Fig. 6). In addition, higher Cu, Zn, Pb and Se content is observed towards the rims of the grain. This increase in base metal content (Cu, Zn and Pb) corresponds to the transition towards the main mineralisation stage, which is characterized by minerals such as chalcopyrite, sphalerite and galena (stage 3 in the paragenesis). This increase could, however, indicate that the outer parts of the stage 2 pyrite form an overgrowth, which already belongs to stage 3. The higher amount of Cu, Pb and Zn in the outer rims of the pyrite grains is locally correlated with the presence

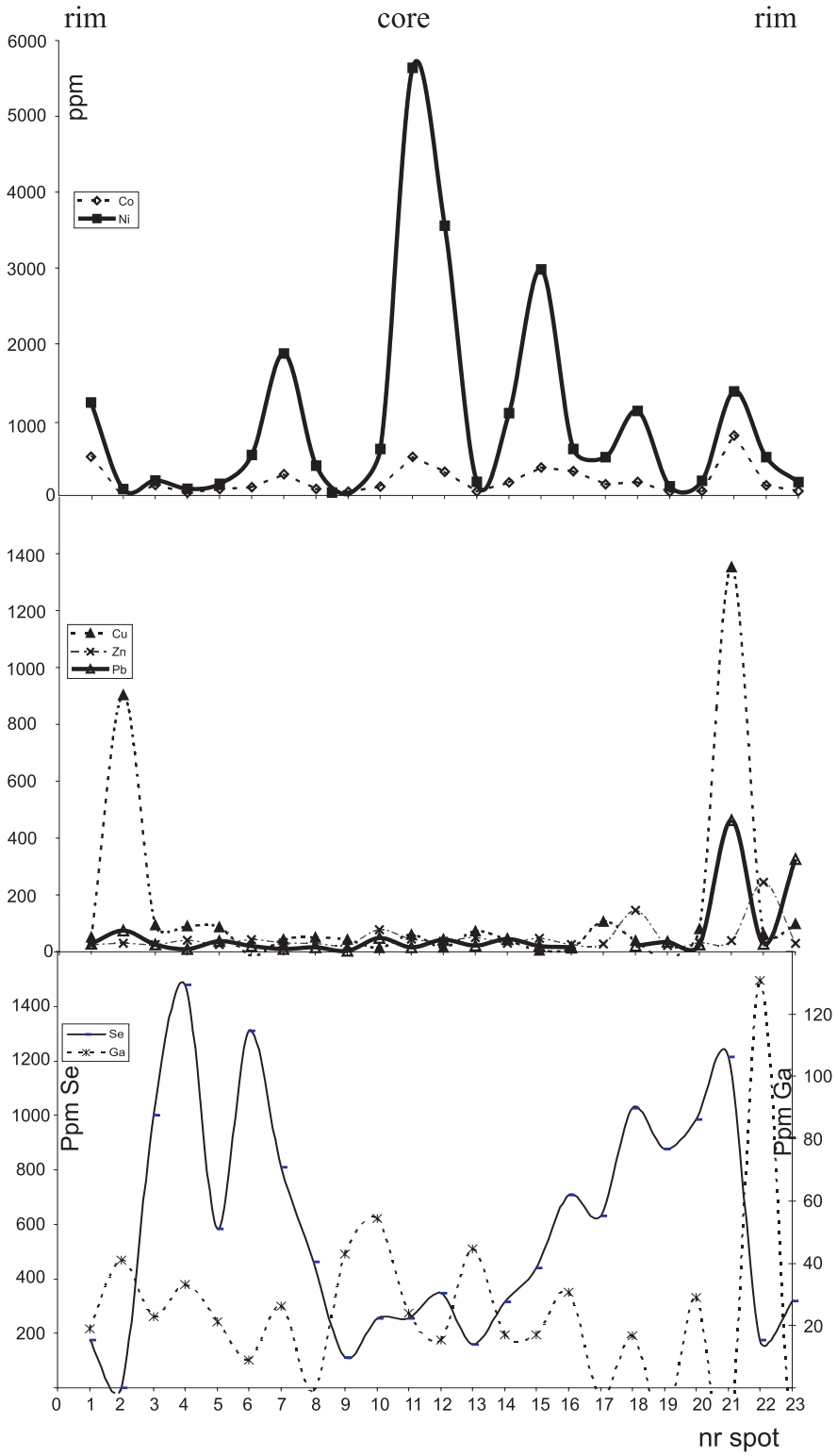

Figure 6. Distribution of trace elements in different spots shot through the pyrite grain. The 23 spots can be seen on Figure 5C.

of mineral inclusions in the outer growth rims (e.g. galena in Fig. 5E). The increase in Se towards the main mineralisation stage has also been observed during electron microprobe measurements. The pyrite from the main stage of the mesozonal mineralisation of the Marcq area is characterised by a higher content of As, Co, Se, Au and Sb (Dewaele *et al*., 2002b; Dewaele & Muchez, 2005). According McCuaig & Kerrich (1998), this is typical for mesozonal mineralisation, which commonly shows a drastic increase of Au and Ag and enrichments of As, Sb, Se, Te, Bi, W, Mo and B.

4. Conclusion

Investigation of the artificially produced sulphide standard for pyrite shows a homogeneity of ≤ 15 percent for the elements Co, Ni, Cu, Ga. The homogeneity is poorer (i.e. RSD > 15%) for Zn, Se and Pb. A relative standard deviation of ≤ 15 percent indicates that the standard is suitable for a (semi-) quantitative characterization of pyrite. Thus, the welding method allows to produce an artificial standard that is applicable for a quick (semi-) quantitative analysis of the elements Co, Ni, Cu and Ga.

The external standard is also useful for qualitative analysis of the elements Zn, Se and Pb. It should be noted that only a limited number of pure elements have been added to the Elba pyrite.

The artificial produced standard has been applied on zoned pyrite from a polysulphide mineralisation. Results are more accurate and there is a lower detection limit compared with electron microprobe analysis. Geochemical trends demonstrate an increase in the Pb, Zn and Cu content towards the rim of the pyrite grain, which is related to the transition to the main stage of the polysulphide mineralisation. An increase of the Se content is also observed, and is also indicated by the increased percentage of significant measurements of electron microprobe analysis (Dewaele *et al*., 2002b; Dewaele & Muchez, 2005).

It, thus, has been illustrated that the method applied can be used to produce matrix-matched external sulphide standards for the LA ICP-MS analysis of sulphides. However, the method applied can definitely be improved by incorporating other trace elements in the matrix of the pyrite/pyrrhotite crystals. In addition, this method should also be tested for other metallic sulphides.

Important shortcomings to the method applied are the welding device, of which the outcome power can only be controlled to a limited extent. No control can be exhibit on the temperature obtained during the welding. Also no control exists on the possible vaporisation of some of the elements during the welding. In addition, only a small amount of reference material is produced by this method.

5. Acknowledgements

Funding was provided by the Fund of Scientific Research of Flanders (F.W.O.-Vlaanderen, Belgium) project G.0274.99. Herman Nijs carefully prepared polished sections. Microprobe analysis were carried out by Jacques Wautier at the Université Catholique de Louvain-La-Neuve. Jean-Clair Duchesne and two anonymous reviewers are greatly thanked for their comment, which strongly improved the text.

References

ARIF, J. & BAKER, T., 2004. Gold paragenesis and chemistry at Batu Hijau, Indonesia: implications for gold-rich porphyry copper deposits. *Mineralium Deposita*, 39: 523-535.

AXELSSON, M.D., 2000. Multi-elemental analysis of geological and biological samples using Laser Ablation ICP SFMS. Unpublished Licentiate thesis, Lulea Techniska Universitet. 77pp.

AXELSSON, M.D. & RODUSHKIN, I., 2001. Determination of major and trace elements in sphalerite using laser ablation double focussing sector field ICP-MS. *Journal of Geochemical Exploration*, 72: 81-89.

BALHAUS, C. & SYLVESTER, P., 2000. Nobel metal enrichment processes in the Merensky Reef, Bushveld Complex. *Journal of Petrology*, 41: 545-561.

BRALIA, A., SABATINI, G. & TROJA, F., 1979. A revaluation of the Co/Ni ratio in pyrite as geochemical tool in ore genesis problems. *Mineralium Deposita*, 14: 353-374.

CAMPBELL, A.J. & HUMAYAN, M., 1999. Trace element microanalysis in iron meteorites by laser ablation ICPMS. *Analyical Chemistry*, 71: 939-946.

CRAIG, J.R., VOKES, F.M. & SOLBERG, T.N., 1998. Pyrite: physical and chemical textures. *Mineralium Deposita*, 34**:** 82-101.

DEWAELE, S. & MUCHEZ, Ph., 2005. Geochemical characteristics of pyrite formed during the evolution of an orogenic fold belt: a case study from the Lower Palaeozoic Anglo-Brabant fold Belt (Belgium). *Transactions of Institution of Mining and Metallurgy (Section B: Applied Earth Sciences)*, 114: 129-137.

DEWAELE, S., BOVEN, A. & MUCHEZ, Ph., 2002a. $^{40}Ar/^{39}Ar$ dating of a mesothermal orogenic low-angle reverse shear zone in the Lower Palaeozoic of the Anglo-Brabant fold belt, Belgium. *Transactions of Institution of Mining and Metallurgy (Section B: Applied Earth Sciences),* 111: 215-220.

DEWAELE, S., MUCHEZ, Ph., BOYCE, DE VOS, W. & WAUTIER, J., 2002b. Trace element and stable isotope geochemistry of pyrites in the Lower Palaeozoic of the Anglo-Brabant fold belt (Belgium): implications for the origin of mineralising fluids. *Aardkundige mededelingen*, 12: 177-180.

DUCHESNE, J.C., ROUHART, A., SCHOUMACHER, C. & DILLEN, H., 1983. Thallium, nickel, cobalt and other trace elements in iron sulphides from Belgian Lead-Zinc Vein deposits. *Mineralium Deposita*, 18**:** 303-313.

EILU, P., MICKUCKI, E.J. & GROVES, D.I., 1997. Wallrock alteration and primary geochemical dispersion in lode-gold exploration. SGA short course series, v. 1, 65p.

FLEET, M.E., CHRYSSOULIS, S.L., MACLEAN, P.J., DAVISDON, R. & WEISENER, C.G., 1993. Arsenian pyrite from gold deposits: Au and As distribution investigated by SIMS and EMP, and color staining and surface oxidation by XPS and LIMS. *The Canadian Mineralogist*, 31**:** 1-17.

FLEET, M.E. & MUMIN, H.A., 1997. Gold bearing arsenian pyrite and marcasite and arsenopyrite from Carlin Trend gold deposits and laboratory synthesis. *The American Mineralogist*, 82**:** 182-193

FOLEY, N., AYUSO, R.A. & SEAL, R.II., 2001. Remnant colloform pyrite at the Haile gold deposit, South Carolina: a textural key to genesis. *Economic Geology*, 96**:** 891-902.

GRIFFEN, W.L., ASHLEY, P.M., RYAN, C.G., SIE S.H. & SUTER, G.F., 1991. Pyrite geochemistry in the North Arm epithermal Ag-Au deposit, Queensland, Australia: a proton-microprobe study. *The Canadian Mineralogist*, 29**:** 185-198.

HALTER,W.E., PETTKE, T. & HEINRICH, C.A., 2004. Laser-ablation ICP-MS analysis of silicate and sulphide melt inclusions in an andestic complex I: analytical approach and data evaluation. *Contributions to Mineralogy and Petrology*, 147**:** 385-396.

HUSTON, D.L., SIE, S.H., SUTER, G.F., COOKE, D.R. & BOTH, R.A., 1995. Trace element in sulphide minerals from eastern Australian VHMS deposits: Part I. Proton microprobe analyses of pyrite, chalcopyrite, and sphalerite, and Part II. Selenium levels in pyrite: Comparison with the $\delta^{34}S$ values and implications for the source of sulphur in volcanogenic hydrothermal systems. *Economic Geology*, 90**:** 1167-1196.

JARVIS, K.E. & WILLIAMS, J.G., 1993. Laser ablation inductively coupled mass spectrometry (LA-ICP-MS): a rapid technique for the direct, quantitative determination of major, trace and rare-earth elements in geological samples. *Chemical Geology*, 106**:** 251-262.

KULLERUD, K. & YODER, H.S., 1959. Pyrite stability relations in the Fe-S system. *Economic Geology*, 54: 533-573

MCCUAIG, T.C. & KERRICH, R., 1998. P-T-t-deformation-fluid characteristics of lode gold deposits: evidence from alteration systematics. *Ore Geology Reviews*, 12**:** 381-453.

MÜLLER, B., AXELSSON, M.D. & ÖHLANDER, B., 2002. Adsorption of trace elements on pyrite surfaces in sulphidic mine tailings from Kristineberg (Sweden) a few years after remediation. *Science of The Total Environment*, 298: 1-16.

NESBITT, R.W., HIRATA, T., BUTLER, I.B. & MILTON, J.A., 1997. UV laser ablation ICP-MS: some applications in the earth sciences. *Geostandards Newsletter*, 21**:** 231-243.

NORMAN, M., ROBINSON, P. & CLARK, D., 2003. Major-and trace element analysis of sulphide ores by laser ablation ICP-MS, solution ICP-MS, and XRF: new data on international reference material. *The Canadian Mineralogist*, 41**:** 293-305.

ØDEGARD, M., 1999. Preparation of synthetic calibration materials for use in the microanalysis of oxide minerals by direct fusion in high-purity graphite electrodes: preliminary results for quartz and rutile. *Geostandards Newsletter*, 23**:** 173-186.

PARR, J., 1994. The preservation of pre-metamorphic colloform banding in pyrite from the Broken-Hill-type Pinnacles deposit, New South Wales, Australia. *Mineralogical Magazine*, 58**:** 461-471.

PIESSENS, K., MUCHEZ, Ph., DEWAELE, S., BOYCE, A., DE VOS, W., SINTUBIN, M., DEBACKER, T., BURKE, E.A.J. & VIAENE, W., 2002. Fluid flow, alteration, and polysulphide mineralisation associated with a low-angle reverse shear zone in the Lower Palaeozoic of the Anglo-Brabant Fold belt, Belgium. *Tectonophysics*, 34**:** 73-92.

PERKINS, W.T., PEARCE, N.J.G. & WESTGATE, J.A., 1997. The development of laser ablation ICP-MS and calibration strategies: examples from the analysis of trace elements in volcanic glass shards and sulphide minerals. *Geostandards Newsletter*, 21**:** 175-190.

RAMDOHR, P. 1969. *The ore minerals and their intergrowths*. Oxford: Pergamon Press.

RAYMOND, O.L., 1996. Pyrite composition and ore genesis in the Prince Lyell copper deposit, Mt. Lyell mineral field, western Tasmania, Australia. *Ore Geology Reviews*, 10**:** 231-250.

RIDLEY, W.I. & LICHTE, F.E., 1998. Major, trace and ultratrace element analysis by Laser Ablation ICP-MS. *In:* McKibben, M.A., Shanks III, W.C., Ridley, W.I. (eds) *Application of mineralogical techniques in understanding mineralizing processes*. Reviews in Economic *Geology,* 7**:** 199-215

ROBINSON, B.W., WARE, N.G. & SMITH, D.G.W., 1998.: Modern electron-microprobe trace-element analysis in mineralogy. *In:* Cabri, L.J., Vaughan, D.J. (eds) *Modern approaches to ore and environmental mineralogy.* Mineralogical Association of Canada, 153-180.

RYALL, W.R., 1977. Anomalous trace elements in pyrite in the vicinity of mineralised zones at Woodlawn, N.S.W., Australia. *Journal of Geochemical Exploration*, 8**:** 73-83.

SHORE, M. & FOWLER, A.D., 1996. Oscillatory zoning in minerals: A Common Phenomenon. *The Canadian Mineralogist*, 34**:** 1111-1126.

WATLING, R.J., HERBERT, H.K. & ABELL, I.D., 1995. The application of laser ablation-inductively coupled plasma-mass spectrometry (LA-ICP-MS) to the analysis of selected sulphide minerals. *Chemical Geology*, 124**:** 67-81.

WILSON, S.A., RIDLEY, W.I. & KOENIG, A.E., 2002. Development of sulphide calibration standards for the laser ablation inductively-coupled plasma mass spectrometry technique. *Joural of Analytical and Atomic Spectrometry*, 17**:** 406-409.

(Manuscript received 01.03.2006; accepted 05.09.2006)